7-5-2023

Estimation of the Kelvin–Helmholtz Unstable Boundary

Xuanye Ma
Embry-Riddle Aeronautical University, max@erau.edu

Scholarly Commons Citation

Ma, X. (2023). Estimation of the Kelvin–Helmholtz unstable boundary. Journal of Geophysical Research: Space Physics, 128, e2023JA031602. https://doi. org/10.1029/2023JA031602

JGR Space Physics

METHOD
10.1029/2023JA031602

Estimation of the Kelvin–Helmholtz Unstable Boundary

Xuanye Ma[1]

[1]Embry–Riddle Aeronautical University, Daytona Beach, FL, USA

Key Points:

- The most Kelvin–Helmholtz (KH) unstable direction can be identified by a matrix
- The range of the KH wave vector direction can be estimated by the eigenvalues
- The matrix also provides a new boundary normal coordinate system

Correspondence to:

X. Ma,
max@erau.edu

Citation:

Ma, X. (2023). Estimation of the Kelvin–Helmholtz unstable boundary. *Journal of Geophysical Research: Space Physics*, *128*, e2023JA031602. https://doi.org/10.1029/2023JA031602

Received 16 APR 2023
Accepted 5 JUL 2023

Abstract The Kelvin–Helmholtz (KH) instability is one of the most important mechanisms of the viscous-like interaction between the solar wind and the magnetosphere (MSP), which transport the mass, energy, momentum, and magnetic flux. Thus, it is important to examine whether the magnetopause boundary is KH unstable or not. Based on the KH onset conditions, this report proposes to use a matrix to identify the most KH unstable direction based on the in situ measurements of the density, velocity, and magnetic field in the MSP and magnetosheath. The range of the KH unstable direction can be easily estimated based on the eigenvalues of the matrix. The eigenvectors of the matrix provide a new boundary normal coordinate system, which could be useful for 2-D KH instability simulation.

1. Introduction

The Kelvin–Helmholtz (KH) instability is a universal physics process in heliophysics (see summary by Johnson et al. (2014) and Masson and Nykyri (2018)). As one of the most important mechanisms of viscous-like interaction between the solar wind and the magnetosphere (MSP), the KH instability can transport the mass, energy, momentum, and magnetic flux (Ma et al., 2014a, 2014b, 2017; Nykyri & Otto, 2001, 2004; Otto, 2006; Otto & Fairfield, 2000; Pu & Kivelson, 1983a, 1983b, 1983c). Thus, it is important to examine whether the magnetopause boundary is KH unstable or not.

Assuming an infinity thin sheared flow boundary width, Chandrasekhar (1961) demonstrated that the KH growth rate, γ, for the incompressible magnetohydrodynamics system is given by

$$\gamma^2 = \alpha_1\alpha_2[(\mathbf{u}_1 - \mathbf{u}_2)\cdot\mathbf{k}]^2 - \alpha_1(\mathbf{v}_{A1}\cdot\mathbf{k})^2 - \alpha_2(\mathbf{v}_{A2}\cdot\mathbf{k})^2, \quad (1)$$

where the subscript 1 and 2 represent the value on each side of the sheared flow boundary layer, $\alpha_i = \rho_i/(\rho_1+\rho_2)$, ρ is the mass density, $\mathbf{u}$ is the bulk velocity, $\mathbf{v}_A = \mathbf{B}/\sqrt{\mu_0\rho}$ is the Alfvén velocity, $\mathbf{B}$ is the magnetic field, μ_0 is the vacuum permeability, and $\mathbf{k}$ is KH wave-vector. Equation 1 reveals that the boundary is KH unstable when $\gamma^2 > 0$. While large flow shear can increase the KH growth rate, the magnetic field in the KH wave-vector direction can stable the KH instability. At the magnetopause boundary, the perturbation often contains the wave vector in all directions, and the KH mode with the largest growth rate becomes the dominant mode. Therefore, the criterion for KH unstable boundary is whether the maximum of Equation 1 is greater than zero. Notice, Equation 1 only contains $\mathbf{k}^2$ term, thus we only need to find the direction which maximizes Equation 1. Such a criterion has often been oversimplified by only examining whether Equation 1 is greater than zero in the specific direction (e.g., shear flow direction), which could largely underestimate the KH insatiability.

Recently, several studies explored the whole 4π solid angle to examine the most KH unstable direction by directly using Equation 1, as well as integration of the total solid angle that satisfies the KH onset conditions as the second reference (Burkholder et al., 2020; Nykyri et al., 2021; Rice et al., 2022). However, this type of examination is computationally expensive, and the accuracy is highly dependent on the wave-vector sample density. Thus, this report will provide a systematic method to find the most KH unstable direction with a well-known technique, the estimation of unstable solid angle will also be simplified to a numerical integration.

2. The Most KH Unstable Direction

Assuming the unperturbed magnetospheric and magnetosheath (MSH) plasma density, bulk velocity, and magnetic field have been identified (e.g., Rice et al., 2022), which are noted by ρ_{MHP}, ρ_{MSH}, $\mathbf{u}_{MHP}$, $\mathbf{u}_{MSH}$, $\mathbf{B}_{MHP}$, and $\mathbf{B}_{MSH}$ in any given coordinate system (e.g., Geocentric Solar Ecliptic system and Geocentric Solar Magnetospheric system), the most KH unstable direction can be identified by using the method of Lagrange multipliers based on

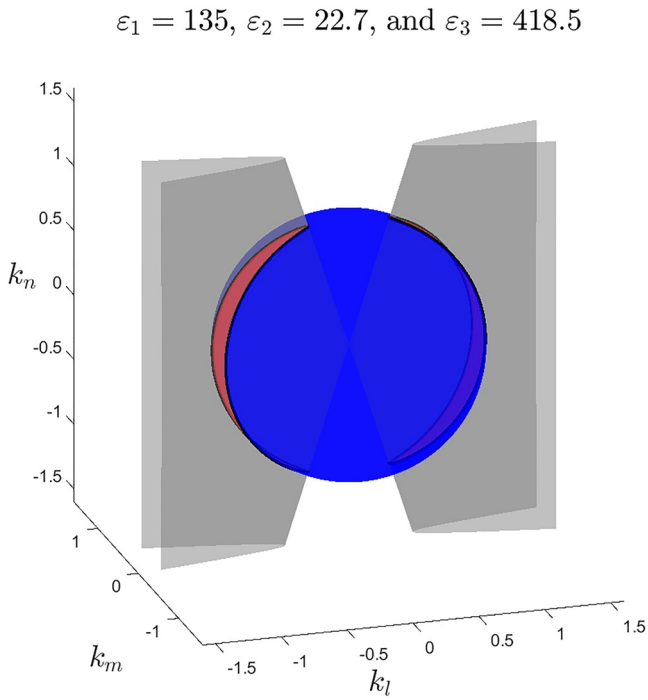

Figure 1. $(\gamma/k)^2$ in the **lmn** coordinate for 8 September 2015 Magnetospheric Multiscale Kelvin–Helmholtz instability event. The gray surface represents $\gamma = 0$, the red area represents the unstable region, and the blue area represents the stable region. The black lines are the boundary between stable and unstable regions.

these boundary conditions, which is exactly the same process as the traditional minimum or maximum variance analysis (MVA) (Sonnerup, 1980). As a demonstration, one can rewrite Equation 1 as

$$\mathcal{L}\left(\hat{\mathbf{k}}, \lambda\right) = (\gamma/k)^2 - \lambda\left(1 - \hat{\mathbf{k}}^2\right) = \left(\mathbf{u}\cdot\hat{\mathbf{k}}\right)^2 - \left(\mathbf{a}_{\mathrm{MSP}}\cdot\hat{\mathbf{k}}\right)^2 - \left(\mathbf{a}_{\mathrm{MSH}}\cdot\hat{\mathbf{k}}\right)^2 - \lambda\left(1 - \hat{\mathbf{k}}^2\right). \tag{2}$$

Here $\mathbf{u} = \sqrt{\alpha_{\mathrm{MSP}}\alpha_{\mathrm{MSH}}}(\mathbf{u}_{\mathrm{MSP}} - \mathbf{u}_{\mathrm{MSH}})$, $\mathbf{a}_i = \sqrt{\alpha_i}\mathbf{v}_{Ai}$, the subscript i represent MSP and MSH, and $\hat{\mathbf{k}}$ is a unit vector. The maximum or minimum of γ/k requires all partial derivatives should be zero, which is given by

$$\frac{\partial\mathcal{L}}{\partial k_x} = \frac{\partial\mathcal{L}}{\partial k_y} = \frac{\partial\mathcal{L}}{\partial k_z} = \frac{\partial\mathcal{L}}{\partial\lambda} = 0. \tag{3}$$

The first three equations in Equation 3 lead to solving three eigenvalues ($\lambda_1 \geq \lambda_2 \geq \lambda_3$) and eigenvectors (**l**, **m**, and **n**) for a 3 × 3 matrix $M_{ij} = u_i u_j - a_{1i}a_{1j} - a_{2i}a_{2j}$, where the subscript i and j represent x, y, and z. (Alternatively, it can be written as $\boldsymbol{M} = \mathbf{uu} - \mathbf{a}_{\mathrm{MSP}}\mathbf{a}_{\mathrm{MSP}} - \mathbf{a}_{\mathrm{MSH}}\mathbf{a}_{\mathrm{MSH}}$ (See Appendix A)).

The maximum eigenvalue λ_1 is the maximum value of $(\gamma/k)^2$, which is along the **l** direction. Thus, the KH unstable sheared flow boundary requires $\lambda_1 > 0$. Notice, Equation 1 is based on the one-dimensional tangential sheared flow boundary geometry, in which $\mathbf{a}_{\mathrm{MSH}}$, $\mathbf{a}_{\mathrm{MSP}}$, and **u** are coplanar. However, for the real observational data, these three vectors can hardly be exactly coplanar. It can be easily shown that in this case, (i.e., $(\mathbf{a}_{\mathrm{MSH}} \times \mathbf{a}_{\mathrm{MSP}})\cdot\mathbf{u} \neq 0$), one can always find a direction (i.e., $\hat{\mathbf{k}} \| \mathbf{a}_{\mathrm{MSH}} \times \mathbf{a}_{\mathrm{MSP}}$) so that $\hat{\mathbf{k}}\cdot\mathbf{a}_{\mathrm{MSH}} = \hat{\mathbf{k}}\cdot\mathbf{a}_{\mathrm{MSP}} = 0$, while $\hat{\mathbf{k}}\cdot\mathbf{a}_{\mathrm{MSH}} = \hat{\mathbf{k}}\cdot\mathbf{u} \neq 0$, indicating that λ_1 must be greater than zero. Therefore, one must check whether the direction of **l** is roughly along the expected direction (see the discussion in Section 5), as well as the range of the KH unstable directions.

Notice, as long as the magnetic fields are not exactly aligned with the sheared flow direction (i.e., $\mathbf{u} \times \mathbf{a}_i \neq 0$), there always exists the direction where the boundary is KH stable (i.e., $\mathbf{u}\cdot\hat{\mathbf{k}} = 0$ and $\mathbf{a}_i\cdot\hat{\mathbf{k}} \neq 0$), which indicates λ_3 must be smaller than zero in this condition.

Considering the case with no magnetic field (i.e., $\mathbf{a}_i = 0$), the sheared flow boundary is KH unstable in almost all the directions (i.e., $\left(\mathbf{u}\cdot\hat{\mathbf{k}}\right)^2 \geq 0$). The equality holds when $\hat{\mathbf{k}}$ is perpendicular to the shear flow direction (i.e., $\mathbf{u} \perp \hat{\mathbf{k}} \rightarrow \left(\mathbf{u}\cdot\hat{\mathbf{k}}\right)^2 = 0$). That is saying, event without any stability effect, one cannot find a plane which $(\gamma/k)^2 > 0$. However, if $\lambda_2 > 0$, then the $(\gamma/k)^2 = \lambda_1 k_l^2 + \lambda_2 k_n^2$ in the **lm** plane is always greater than zero, which is not possible. Thus, λ_2 must be smaller or equator to zero.

In summary, as long as the magnetic field is not exactly aligned with the flow shear, the eigenvalues of matrix $\boldsymbol{M}$ have to be $\lambda_1 > 0 \geq \lambda_2 \geq \lambda_3$, in which λ_1 is the maximum value of $(\gamma/k)^2$, and associated eigen-vector **l** is the most KH unstable direction. The other two eigenvalues are smaller than zero, which indicates that the boundary is KH stable along the directions of the associated eigenvectors (i.e., **m**, and **n** direction).

3. KH Unstable Solid Angle

Based on the above discussion, assuming a KH unstable boundary with $\lambda_1 = \varepsilon_1^{-2}$, $\lambda_2 = -\varepsilon_2^{-2}$, and $\lambda_3 = -\varepsilon_3^{-2}$, the growth rate γ in the eigenvectors coordinate system (**lmn**) can be represented as a quadratic form $\gamma^2 = (k_l/\varepsilon_1)^2 - (k_m/\varepsilon_2)^2 - (k_n/\varepsilon_3)^2$, which is an elliptic hyperboloid of two sheets (see Figure 1). Thus, the total unstable solid angle is the area of the cross-section between the elliptic hyperboloid of two sheets ($\gamma \geq 0$, gray surface in Figure 1) and unit sphere $\left(k_l^2 + k_m^2 + k_n^2 = 1\right)$, which is bounded by elliptic curves: $1 = (k_m/A)^2 + (k_n/B)^2$ (black lines in Figure 1). Here, $A^2 = \frac{|\lambda_1|}{|\lambda_1|+|\lambda_2|} < 1$, and $B^2 = \frac{|\lambda_1|}{|\lambda_1|+|\lambda_3|} < 1$. Rewritten the k_l, k_m, and k_n in a sphere coordinate, (i.e., $k_l = \cos\theta$, $k_m = \sin\theta\cos\varphi$, $k_n = \sin\theta\sin\varphi$), the total unstable solid

angle is given by a surface integral $\Omega = 2\int_0^{2\pi}\int_0^{\theta_1}\sin\theta d\theta d\varphi$, which is bounded by the elliptic curves: $k_m = A\sin\phi = \sin\theta_1\cos\varphi$, $k_n = B\cos\phi = \sin\theta_1\sin\varphi$, and $k_l = \cos\theta_1 = \sqrt{1 - A^2\sin^2\phi - B^2\cos^2\phi}$. This surface integral can be simplified to a one-variable integral

$$\Omega = 4\pi - 8\int_0^{\pi/2}\sqrt{\frac{\sin^2\varphi + a}{\sin^2\varphi + b}}d\varphi, \tag{4}$$

where $a = \frac{|\lambda_2|}{(|\lambda_3| - |\lambda_2|)}$, and $b = \frac{(|\lambda_1| + |\lambda_2|)}{(|\lambda_3| - |\lambda_2|)}$. In principle, Equation 4 can be further represented by using elliptic functions. However, it does not bring more numerical convenience compared to direct numerical integration of Equation 4.

Sometimes, researchers prefer to determine the normal direction by using traditional boundary normal analysis methods (e.g., MVA method see discussion by Ma et al. (2016)). Based on the one-dimensional tangential discontinuity assumption, the normal direction of the magnetic field and velocity is expected to be zero. Thus, we have $\lambda_2 \approx 0$, and the nonzero growth rate requires $(\gamma/k)^2 = \lambda_1\cos^2\theta_k + \lambda_3\sin^2\theta_k \geq 0$, where θ_k is the angle between unit wave vector $\hat{\mathbf{k}}$ and $\mathbf{l}$. which yield the total unstable angle equates $4\theta_c$, where $\cos\theta_c = \sqrt{|\lambda_3|/(|\lambda_1| + |\lambda_3|)}$. Notice, for a marginal KH unstable boundary, λ_1 is expect to be small (i.e., $|\lambda_1| \ll |\lambda_3|$), which yields $\theta_c \approx 0$, being consistent with what we would expect. The same results can also be archived by integrating Equation 4 with $a = 0$, which gives $\Omega = 8\theta_c$. Notice, in this case, the results should be normalized by the whole solid angle, which is 4π instead of 2π for two-dimensional (2-D) geometry.

4. Example

On 8 September 2015, the four Magnetospheric Multiscale spacecraft observed KH waves at the duskside magnetopause (Eriksson et al., 2016), in which $n_{MSP} = 5.7$, $n_{MSH} = 20.1\ \mathrm{cm}^{-3}$, $\mathbf{u}_{MSP} = (-0.7, 16.6, -1.0)$, $\mathbf{u}_{MSH} = (-355.9, 16.6, -1.0)$ km s^{-1}, $\mathbf{B}_{MSP} = (5.5, 5.3, 63.4)$, and $\mathbf{B}_{MSH} = (24.3, -1.5, 71.1)$ nT in the maximum flow shear system coordinate (see Table S3 in Supporting Information of Eriksson et al. (2016)). Thus, $\mathbf{u} = (147.4, 0, 0)$, $\mathbf{a}_{MSP} = (23.6, 22.7, 272.1)$, $\mathbf{a}_{MSH} = (104.3, -6.4, 305.2)$ km s^{-1}, which yields

$$\boldsymbol{M} = 10^5 \times \begin{pmatrix} 0.1028 & 0.0013 & -0.3825 \\ 0.0013 & -0.0056 & -0.0423 \\ -0.3825 & -0.0423 & -1.6716 \end{pmatrix} \mathrm{km^2 s^{-2}}.$$

The three eigenvalues of $\boldsymbol{M}$ are $\lambda_1 = \left(135\,\mathrm{km\,s^{-1}}\right)^2$, $\lambda_2 = -\left(22.7\,\mathrm{km\,s^{-1}}\right)^2$, and $\lambda_3 = -\left(418.5\,\mathrm{km\,s^{-1}}\right)^2$, and the associated three eigenvectors are $\mathbf{l} = (0.978, 0.053, -0.203)$, $\mathbf{m} = (-0.056, 0.998, -0.0124)$, and $\mathbf{n} = (0.202, 0.024, 0.979)$ in the maximum flow shear system coordinate. The total unstable solid angle is $\Omega = 2.4$, and for 2-D assumption, $\theta_c = 17.9°$. Notice, the $\mathbf{l}$ is mostly along the sheared flow direction, the $\mathbf{m}$ is mainly along the magnetopause normal direction, and the $\mathbf{n}$ is roughly along the north direction. This **lmn** coordinate system is mainly consistent with the maximum flow shear system, suggesting for this specific case the most KH unstable direction happens to be close to the shear flow direction. This is because in this case, the sheared flow is mostly perpendicular to the magnetic field, and the Alfvén speed associated with the magnetic field is large.

5. Summary and Caveat

Based on the KH onset conditions (i.e., Equation 1), this report proposes to use a matrix $\boldsymbol{M} = \mathbf{uu} - \mathbf{a}_{MSP}\mathbf{a}_{MSP} - \mathbf{a}_{MSH}\mathbf{a}_{MSH}$ to identify the most KH unstable direction based on the in situ measurements of the density, velocity, and magnetic field in the MSP and MSH. The largest eigenvalue of matrix $\boldsymbol{M}$, $\lambda_1 \geq 0$, represents the possibly largest $(\gamma/k)^2$, and its eigenvector $\mathbf{l}$ represents the most unstable direction. Although this direction is expected to be mostly in the sheared flow direction, it is possible that $\mathbf{l}$ points to the north if the magnetic field is mainly aligned with the sheared flow direction. Thus, one may set a critical angle θ_{max}, that the angle between $\mathbf{l}$ and the equatorial plane must be smaller than θ_{max} for the KH unstable sheared flow boundary. The value of the critical angle, θ_{max} should be determined based on the local magnetopause geometry.

For instance, the shape and size of the Earth's magnetopause can be well described in a functional form, $r = r_0[2/(1 + \cos\phi)]^{\alpha}$, where the value r is the radial distance at an angle ϕ between the Sun-Earth line and the radial direction, r_0 and α are the functions of the interplanetary magnetic field B_z and solar wind dynamic pressure D_p, representing the standoff distance and the level of tail flaring, respectively (Shue et al., 1997). For any given ϕ (or equivalently local time), the typical length scale along the magnetopause tangential direction can be represented by the radius of curvature of the magnetopause shape function,

$$R = \frac{\left[(r')^2 + r^2\right]^{3/2}}{2(r')^2 - rr'' + r^2},$$

where $r' = dr/d\phi$, $r'' = dr'/d\phi$ (Carmo, 2018). Meanwhile, the typical length scale along the z direction can be estimated by the magnetopause distance $L_z = r\sin\phi$. Thus, the angle between the KH wave vector direction and the equatorial plane θ should be smaller than $\theta_{\max} = \arctan(L_z/R)$. For the solar wind conditions that the model has been valid, (i.e., $-18 < B_z < 15$ nT, and $0.5 < D_p < 8.5$ nPa (Shue et al., 1998)), $\theta_{\max}$ is in a range between 20° and 32° near the magnetopause flank region. Meanwhile, for the marginal KH unstable case, λ_1 is expected to be small. Thus, one can also use the local typical speeds (e.g., sounds speed, Alfvén speed, or fast mode speed) as a reference. Alternatively, the θ_c, being a function of λ_1/λ_3, is another good quantity to examine the stability of the sheared flow boundary.

This report also provides a numerical integration to estimate the total unstable solid angle Ω. Intuitively, a smaller Ω indicates a strong stability effect. But it could also be because that the three vectors, $\mathbf{a}_{\mathrm{MSH}}$, $\mathbf{a}_{\mathrm{MSP}}$, and $\mathbf{u}$ are mostly coplanar (i.e., small $|\lambda_2|$). For this case, the unstable angle $4\theta_c$ is more suitable to describe the range of the KH wave vector. Nevertheless, as we have pointed out $\Omega/4\pi = 4\theta_c/2\pi$, for the limitation case that $\lambda_2 = 0$. Thus, it is recommended to use $\Omega/4\pi$ as a more general quantity to represent the range of the possible KH unstable directions.

The byproduct of this study is a new boundary normal coordinate system (i.e., **lmn**), in which the **m** direction can be treated as the normal direction. The assumption is that the **m** direction is mostly perpendicular to the sheared flow as well as the magnetic fields, which leads $|\lambda_2|$ close to zero. Thus, the ratio of $|\lambda_2|/\max(|\lambda_1|, |\lambda_3|)$ can be used to identify the robustness of this coordinate system. Such a coordinate system is useful for 2-D KH instability simulation, in which the KH wave vector should be in the simulation plane (e.g., Otto & Fairfield, 2000). Notice, the normal directions from different boundary normal analysis methods are based on their own assumption of the boundary layer (e.g., rotational discontinuity or tangential discontinuity). Although different methods should give similar results, there is no perfect analysis method to fit all the conditions. One should choose the method or assumption that most fit the plausible physics process.

Equation 1 demonstrates that a short KH-wavelength mode has a faster growth rate (i.e., $\gamma \propto k$) for a tangential sheared flow. However, for a sheared flow with a finite initial width of Δ, it has been shown that only modes with $k\Delta < 2$ are unstable and the fastest growing modes occur for $k\Delta \sim 0.5$ to 1 (Miura, 1982). In the magnetopause, the width of sheared flow is determined by the kinetic-scale diffusion process. Therefore, the value of Δ is close to the ion inertial length or the ion gyroradius, (i.e., about tens to hundreds of kilometers in the Earth's magnetopause), which is much smaller than the typical KH wavelength in the Earth's magnetopause (i.e., two to six Earth's radii). Thus, the assumption of Equation 1 is still applicable to the Earth's MSP.

Appendix A: Derivation of *M* from Equation 3

Notice for any vector $\mathbf{f}$, $\partial_{k_i}\left[\left(\mathbf{f}\cdot\hat{\mathbf{k}}\right)^2\right] = \partial_{k_i}(f_xk_x + f_yk_y + f_zk_z)^2 = 2(f_xk_x + f_yk_y + f_zk_z)f_i = 2\left(\mathbf{f}\cdot\hat{\mathbf{k}}\right)f_i$, thus Equation 3 can be rewritten as:

$$\partial_{k_i}\mathcal{L} = 2\left(\mathbf{u}\cdot\hat{\mathbf{k}}\right)u_i - 2\left(\mathbf{a}_{\mathrm{MSP}}\cdot\hat{\mathbf{k}}\right)a_{\mathrm{MSP}_i} - 2\left(\mathbf{a}_{\mathrm{MSH}}\cdot\hat{\mathbf{k}}\right)a_{\mathrm{MSH}_i} - 2\lambda\left(\hat{\mathbf{k}}\cdot\hat{\mathbf{k}}\right)k_i = 0.$$

Since $\hat{\mathbf{k}}\cdot\hat{\mathbf{k}} = \mathbf{1}$, the above equation can be further simplify as:

$$\left(\mathbf{u}\cdot\hat{\mathbf{k}}\right)\mathbf{u} - \left(\mathbf{a}_{\mathrm{MSP}}\cdot\hat{\mathbf{k}}\right)\mathbf{a}_{\mathrm{MSP}} - \left(\mathbf{a}_{\mathrm{MSH}}\cdot\hat{\mathbf{k}}\right)\mathbf{a}_{\mathrm{MSH}} - \lambda\hat{\mathbf{k}} = 0$$

$$(\mathbf{uu} - \mathbf{a}_{\mathrm{MSP}}\mathbf{a}_{\mathrm{MSP}} - \mathbf{a}_{\mathrm{MSH}}\mathbf{a}_{\mathrm{MSH}} - \lambda\boldsymbol{I})\cdot\hat{\mathbf{k}} = 0,$$

which is the eigenvalue equation for matrix $\boldsymbol{M} = \mathbf{uu} - \mathbf{a}_{\mathrm{MSP}}\mathbf{a}_{\mathrm{MSP}} - \mathbf{a}_{\mathrm{MSH}}\mathbf{a}_{\mathrm{MSH}}$.

Data Availability Statement

All observational data in the example are based on Table 3 of Supporting Information by Eriksson et al. (2016).

Acknowledgments
The author would like to acknowledge NASA funding: 80NSSC18K1108, 80NSSC22K0304, 80NSSC18K1381, DOE funding: GC87041, and NSF funding: 2308853. The author would also like to thank his parents Zhansheng Ma and Wei Li for their encouragement during this study.

References

Burkholder, B. L., Delamere, P. A., Johnson, J. R., & Ng, C. (2020). Identifying active Kelvin–Helmholtz vortices on Saturn's magnetopause boundary. *Geophysical Research Letters*, *47*(1), e2019GL084206. https://doi.org/10.1029/2019GL084206

Carmo, M. P. D. (2018). *Differential geometry of curves & surfaces* (Revised & updated second edition ed.). Dover Publications, INC.

Chandrasekhar, S. (1961). *Hydrodynamic and hydromagnetic stability*. Dover Publ. Retrieved from http://books.google.com/books?id=oU_-6ikmidoC

Eriksson, S., Lavraud, B., Wilder, F. D., Stawarz, J. E., Giles, B. L., Burch, J. L., et al. (2016). Magnetospheric Multiscale observations of magnetic reconnection associated with Kelvin-Helmholtz waves. *Geophysical Research Letters*, *43*(11), 5606–5615. https://doi.org/10.1002/2016GL068783

Johnson, J., Wing, S., & Delamere, P. (2014). Kelvin Helmholtz instability in planetary magnetospheres. *Space Science Reviews*, *184*(1–4), 1–31. https://doi.org/10.1007/s11214-014-0085-z

Ma, X., Delamere, P., Otto, A., & Burkholder, B. (2017). Plasma transport driven by the three-dimensional Kelvin-Helmholtz instability. *Journal of Geophysical Research: Space Physics*, *122*(10), 10382–10395. https://doi.org/10.1002/2017JA024394

Ma, X., Otto, A., & Delamere, P. A. (2014a). Interaction of magnetic reconnection and Kelvin-Helmholtz modes for large magnetic shear: 1. Kelvin-Helmholtz trigger. *Journal of Geophysical Research: Space Physics*, *119*(2), 781–797. https://doi.org/10.1002/2013ja019224

Ma, X., Otto, A., & Delamere, P. A. (2014b). Interaction of magnetic reconnection and Kelvin-Helmholtz modes for large magnetic shear: 2. Reconnection trigger. *Journal of Geophysical Research: Space Physics*, *119*(2), 808–820. https://doi.org/10.1002/2013ja019225

Ma, X., Otto, A., Delamere, P. A., & Zhang, H. (2016). Interaction between reconnection and Kelvin-Helmholtz at the high-latitude magnetopause. *Advances in Space Research*, *58*(2), 231–239. https://doi.org/10.1016/j.asr.2016.02.025

Masson, A., & Nykyri, K. (2018). Kelvin-Helmholtz instability: Lessons learned and ways forward. *Space Science Reviews*, *214*(4), 71. https://doi.org/10.1007/s11214-018-0505-6

Miura, A. (1982). Nonlinear evolution of the magnetohydrodynamic Kelvin-Helmholtz instability. *Physical Review Letters*, *49*(11), 779–782. https://doi.org/10.1103/physrevlett.49.779

Nykyri, K., Ma, X., Burkholder, B., Rice, R., Johnson, J. R., Kim, E., et al. (2021). MMS observations of the multiscale wave structures and parallel electron heating in the vicinity of the southern exterior cusp. *Journal of Geophysical Research: Space Physics*, *126*(3), e2019JA027698. https://doi.org/10.1029/2019ja027698

Nykyri, K., & Otto, A. (2001). Plasma transport at the magnetospheric boundary due to reconnection in Kelvin-Helmholtz vortices. *Geophysical Research Letters*, *28*(18), 3565–3568. https://doi.org/10.1029/2001GL013239

Nykyri, K., & Otto, A. (2004). Influence of the Hall term on KH instability and reconnection inside KH vortices. *Annales Geophysicae*, *22*(3), 935–949. https://doi.org/10.5194/angeo-22-935-2004

Otto, A. (2006). Mass transport at the magnetospheric flanks associated with three-dimensional Kelvin-Helmholtz modes. In *AGU fall meeting abstracts* (Vol. 2006, p. SM33B–0365).

Otto, A., & Fairfield, D. H. (2000). Kelvin-Helmholtz instability at the magnetotail boundary: MHD simulation and comparison with Geotail observations. *Journal of Geophysical Research*, *105*(A9), 21175–21190. https://doi.org/10.1029/1999JA000312

Pu, Z.-Y., & Kivelson, M. G. (1983a). Kelvin-Helmholtz Instability at the magnetopause: Energy flux into the magnetosphere. *Journal of Geophysical Research*, *88*(A2), 853–861. https://doi.org/10.1029/JA088iA02p00853

Pu, Z.-Y., & Kivelson, M. G. (1983b). Kelvin-Helmholtz instability at the magnetopause. I - Solution for compressible plasmas. II - Energy flux into the magnetosphere. *Journal of Geophysical Research*, *88*(A2), 841–861. https://doi.org/10.1029/ja088ia02p00841

Pu, Z.-Y., & Kivelson, M. G. (1983c). Kelvin-Helmholtz instability at the magnetopause: Solution for compressible plasmas. *Journal of Geophysical Research*, *88*(A2), 841–852. https://doi.org/10.1029/JA088iA02p00841

Rice, R. C., Nykyri, K., Ma, X., & Burkholder, B. L. (2022). Characteristics of Kelvin–Helmholtz waves as observed by the MMS from September 2015 to March 2020. *Journal of Geophysical Research: Space Physics*, *127*(3), e2021JA029685. https://doi.org/10.1029/2021JA029685

Shue, J.-H., Chao, J. K., Fu, H. C., Russell, C. T., Song, P., Khurana, K. K., & Singer, H. J. (1997). A new functional form to study the solar wind control of the magnetopause size and shape. *Journal of Geophysical Research*, *102*(A5), 9497–9511. https://doi.org/10.1029/97JA00196

Shue, J.-H., Song, P., Russell, C. T., Steinberg, J. T., Chao, J. K., Zastenker, G., et al. (1998). Magnetopause location under extreme solar wind conditions. *Journal of Geophysical Research*, *103*(A8), 17691–17700. https://doi.org/10.1029/98JA01103

Sonnerup, B. U. O. (1980). Theory of the low-latitude boundary layer. *Journal of Geophysical Research*, *85*(A5), 2017–2026. https://doi.org/10.1029/JA085iA05p02017